Available online at www.sciencedirect.com

jmr&t Journal of Materials Research and Technology

journal homepage: www.elsevier.com/locate/jmrt

Characterization approaches affect asymmetric load predictions of hexagonal close-packed alloy

V. Tuninetti [a,*], A. Oñate [b,c], M. Valenzuela [d], H. Sepúlveda [e], G. Pincheira [f], C. Medina [g], C. García-Herrera [h], L. Duchêne [i], A.M. Habraken [i,j]

[a] Department of Mechanical Engineering, Universidad de La Frontera, Temuco 4780000, Chile
[b] Department of Materials Engineering, Universidad de Concepción, Concepción 4030000, Chile
[c] Departamento de Ingeniería Mecánica, Facultad de Ingeniería, Universidad del Bío-Bío, 4051381 Concepción, Chile
[d] Doctoral Program in Sciences of Natural Resources, Universidad de La Frontera, Casilla 54-D, Temuco 4780000, Chile
[e] Magíster en Ciencias de la Ingeniería, Universidad de La Frontera, Temuco, Chile
[f] Department of Industrial Technologies, Universidad de Talca, Curicó 3344158, Chile
[g] Department of Mechanical Engineering (DIM), Faculty of Engineering, Universidad de Concepción, Edmundo Larenas 219, Concepción 4030000, Chile
[h] Departamento de Ingeniería Mecánica, Universidad de Santiago de Chile, Santiago 9170022, Chile
[i] Department ArGEnCo-MSM, University of Liège, Liège 4000, Belgium
[j] Fonds de la Recherche Scientifique—F.R.S.-F.N.R.S., Brussels 1000, Belgium

ARTICLE INFO

Article history:
Received 15 May 2023
Accepted 26 August 2023
Available online 30 August 2023

Keywords:
Plastic instability
Identification strategy
Tension-compression asymmetry
hcp

ABSTRACT

The anisotropic plasticity constants of the CPB06 criterion for Ti64, previously identified with experiments performed in all three dimensions, are applied here to evaluate the effect of the direct and inverse calibration strategies of the tensile-compression asymmetry parameter k on the predictive behavior of large deformations of the hexagonal close-packed (hcp) alloy. The direct calibration strategy is based on model fitting with experimental strain hardening data up to the onset of plastic instability. The inverse calibration strategy reduces prediction errors of the load-displacement curves of both the cylindrical bar tensile and the elliptical cylinder compression tests. The results provide interesting insights into the identification of the laws modeling large deformations of hcp materials.

1. Introduction

The accurate prediction of the large deformations process of metals and alloys is of current interest to materials scientists and mechanical designers working in Industry 4.0. Recently, several types of applications have been developed relating to optimization [1–7], advanced manufacturing techniques [8–13] and advances in mechanical properties [14–21]. In particular, for optimizing advanced Ti64 fabrication processes, Racz et al. [11]investigated the optimal fabrication method of Ti64 for cranioplasty due to its excellent formability and biocompatibility characteristics. In Bambach et al. [22] the incorporation of hybrid Ti64 processing technologies combining wire arc additive manufacturing (WAAM) and forging was carried out for the production of complex parts requiring multiple forging steps. This resulted in a solid metallurgical bond in the transition zone, reducing potential damage under loading conditions compared to the traditional process. In addition, they found that with this hybrid

* Corresponding author.
E-mail address: victor.tuninetti@ufrontera.cl (V. Tuninetti).
https://doi.org/10.1016/j.jmrt.2023.08.255

processing method it was possible to substantially increase the mechanical properties of the material by incorporating a subsequent heat treatment.

The mechanical response of Ti64 alloy, when processed by different fabrication methods is complex due to the lack of isotropy, as demonstrated by Huang et al. [23] when evaluating the mechanical response of the material processed by selective laser melting. Since the load response of this alloy includes anisotropy and tensile/compression asymmetry, the latter being of major significance [24,25], simulating the large plastic behavior of this material is challenging.

The complexity of hcp metals and alloys has been investigated by several authors in order to characterize the mechanical behavior for bulk and sheet metal forming processes, additive manufacturing, and parts design under operational conditions of combined stress states [26–31]. The local behavior of this hexagonal close-packed (hcp) material is governed by complex sliding phenomena and twinning, with the consequent tension-compression asymmetry (also called differential strength effect) [32]. Therefore, to perform accurate simulations and optimize the large deformation processes, both the yield surface based on a plasticity criterion and the strain hardening law must be defined and accurately identified.

The plasticity criterion of CPB06 has been widely applied to Ti64 in several studies, thus demonstrating that the experimental points of the yield surface can be well described [33–36]. However, selecting the correct identification strategy for strain hardening law is not always clearly established. This identification can be made by using either direct methods based on information obtained from experimental tensile and compression stress-strain curves or by using finite element simulations of the tests evaluated in the broad plasticity domain, including plastic instability phenomena, also called inverse identification.

In this work, we quantify the effect of the calibration approaches on the prediction accuracy of the tension-compression asymmetric hardening behavior of a hcp Ti64 at large deformation including plastic instability. We provide new insights and findings from successful compression and plane strain simulations and numerical results of plastic instability in cylindrical tensile samples that support the hypothesis: "The selection of calibration approach affects the asymmetric load predictions of hcp alloy". The finite element (FE) material model selected to simulate the evolving quasi-static, anisotropic, and tension-compression asymmetric mechanical response until the onset of fracture of bulk Ti64 alloy is based on five distorted CPB06 plasticity surfaces [25]. While the other directions are modelled by distortional hardening, the model considers that the different yielding surfaces follow the nonlinear strain hardening response of Voce in the reference direction of the alloy. The two identification methods performed and compared are direct and inverse. These two strategies are evaluated considering the ability to predict loads over the entire elastoplastic range, particularly in the large deformation zone including strain levels higher than plastic instability or localized necking. The direct identification is performed by curve fitting of the model with the actual stress vs. logarithmic strain data from tensile tests under uniform stress states, without considering data generated during necking or under triaxial stress states. The second identification strategy consists of minimizing the load prediction error obtained in the test simulations compared to the experimental data generated until the strain levels of complete failure of the tensile specimen. By considering more information in the second strategy, greater accuracy in the predictions is expected; however, it is difficult to establish suitable model parameters given the complexity of the identification due to the asymmetry of the mechanical response in terms of strain hardening between tension and compression.

In the following sections, the methods and main results obtained with the two-calibration strategy of the CPB06 asymmetry parameter k and strain hardening are reported, including the assessment of the two identification methods and their influence on the predictive behavior of the CPB06-Ti64 plasticity model at the large strain level. The accurately identified plasticity coefficient C_{ij} from inverse modeling with experimental data restricted until plastic instability reported by Tuninetti et al. [25] are keep constant here for both identification strategies, given that the focus is to quantify only the effect of asymmetric strength and strain hardening-related parameters.

In this context, the main aim of this study is to compare the effect of identification methods for the hardening and the k-parameter, which are responsible for predicting the tension-compression asymmetry of the plasticity model.

Section 2 defines the asymmetric behavior of Ti64 described by the CPB06 plasticity model and details the two applied calibration strategies. Section 3 provides the prediction results, assessment and analysis of the identification methods for tensile, compressive and plane strain states. Finally, the main findings drawn from this work are given in Section 4.

2. Materials and methods

2.1. The Ti64 asymmetric behavior described by CPB06

The orthotropic plastic behavior of Ti64 is described by 5 previously identified distorted CPB06 yielding surfaces characterized in Ref. [25]. The asymmetric tension-compression hardening behavior is adjusted in this work by a k-parameter of the CPB06 criterion and the constants of the Voce law representing the reference tensile hardening. The CPB06 equivalent stress for the studied Ti64 is given in Eq. (1).

$$\sigma^{\mathrm{CPB06}} = \tilde{m}\left\{\left(|\Sigma_1| - k\,\Sigma_1\right)^2 + \left(|\Sigma_2| - k\,\Sigma_2\right)^2 + \left(|\Sigma_3| - k\,\Sigma_3\right)^2\right\}^{\frac{1}{2}}. \quad (1)$$

$\Sigma_1, \Sigma_2, \Sigma_3$ are the principal values of the tensor $\Sigma = \mathbf{C} : \mathbf{S}$, where $\mathbf{C}$ is the orthotropy tensor and $\mathbf{S}$ is the deviator of the Cauchy tensor. In this study, C_{ij} parameters mainly affecting the shape of the yield surface are values previously tuned for the anisotropy behavior of the alloy [25]. The material constant $\tilde{m}$ describes the equivalent stress as the tensile hardening in the reference direction. The Voce-type isotropic hardening law given in Eq. (2) was chosen to compute the stress tensile stress (σ) in terms of equivalent plastic strain $(\bar{\varepsilon}_p)$:.

$$\sigma\left(\bar{\varepsilon}_p\right) = A + B\left[1 - \exp\left(-C\bar{\varepsilon}_p\right)\right] \quad (2)$$

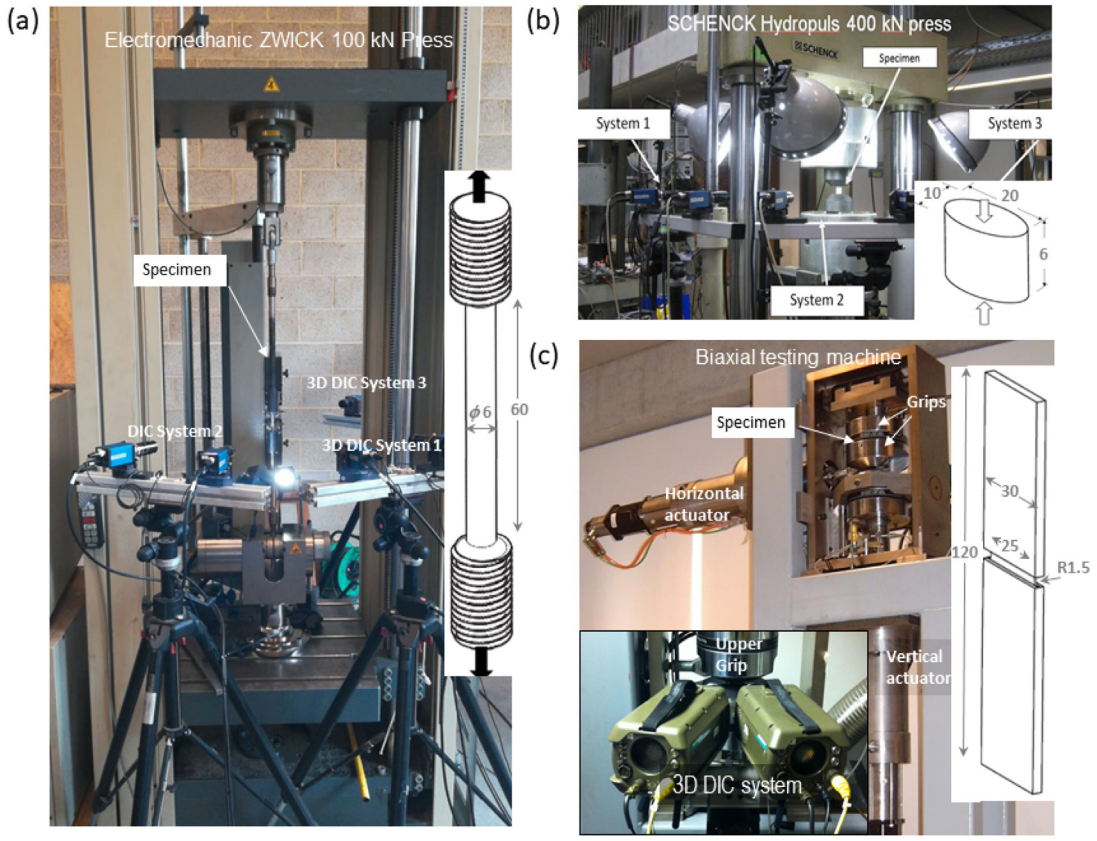

Fig. 1 – Mechanical experiments: machines, measurement devices, and dimensions of the samples. (a) Tensile of cylindrical bar, (b) compression of elliptical cylinder, and (c) plane strain tensile.

A represent the stress at the onset of yielding, while *B* and *C* represent the stagnation and hardening rate, respectively.

2.2. *Definition of the identification approaches investigated*

The anisotropic plasticity parameters given in Table 1 and applied to the CPB06 model have been previously identified with mechanical experiments performed in the three dimensions of the alloy [25]. To determine the two sets of constitutive hardening parameters with the investigated direct and inverse identification strategies, tension and compression tests data are post-processed according to the procedure described in Tuninetti et al. [35]. The performed tests selected for the identification are the tensile of the cylindrical bar (Fig. 1a), compression of the elliptical cylinder (Fig. 1b) and the plane strain tensile (Fig. 1c). The tensile test provides the reference hardening parameters from the experimental stress-strain relation for direct identification or from load-displacement for the inverse approach, mainly because the highest strain values are reached with this sample before the fracture occurs. The compression test adjusts the asymmetry *k*-value while the plane strain assesses the calibration approaches for sheet metal forming applications. Further details of the experimental arrangement of machines and measurement devices as well as the dimensions of the samples are given in Fig. 1. The loading conditions include a controlled non-constant machine head speed computed with the method described in Ref. [37] for a constant deformation rate of 0.001 s^{-1}. This method is required for providing accurate experimental data with no effect of strain rate variations on the strain hardening or tension compression asymmetry evolution. The determined model constants are provided in Table 1.

Table 1 – Anisotropic model constant (C_{ij}) as a function of the specific plastic strain energy [35].

Strain energy per unit volume (W/m3)	Anisotropic constants of CPB06						
	C_{11}	C_{12}	C_{13}	C_{22}	C_{23}	C_{33}	C_{44}=C_{55}=C_{66}
1.86	1	−2.37	−2.36	−1.84	1.20	−2.44	−3.61
9.38	1	−2.50	−2.93	−2.28	1.28	−2.45	4.02
48.6	1	−2.43	−2.92	1.65	−2.24	1.00	−4.00
100	1	−2.57	−2.88	1.39	−2.38	0.88	−3.93
207	1	−2.97	−2.93	0.53	−2.96	0.44	−3.88

Table 2 – Identified model parameters for asymmetric hardening with direct and inverse identification methods [38].

	k-value for yield surfaces at a specific plastic strain energy levels (W/m^3)					Strain hardening coefficients		
	1.857	9.377	48.66	100.2	206.6	A	B	C
Direct	−0.136	−0.136	−0.165	−0.164	−0.18	921	160	15.5
Inverse	−0.136	−0.136	−0.125	−0.114	−0.11	918	290	5.8

The direct and inverse identification strategies investigated here directly influence the k-value of the tension/compression asymmetry from the CPB06 criterion and the reference tensile hardening constants from the Voce's law. The first identification strategy is mainly based on the experimental actual stress-strain data until the necking point computed with the Considère criterion (CPB06 direct), and the second is performed by reducing the FE prediction errors of load-displacement curves of both the tensile test of a cylindrical bar and the compression test of an elliptical cylinder sample. The latter strategy allows to obtain a model called here CPB06 (inverse). Digital image correlation has been applied to all the experiments to evaluate the two identification strategies and cross-sectional area prediction model capabilities. Note that the anisotropic shape evolution of the cross-section is not evaluated here, as this behavior is mainly driven by the previously determined anisotropic constants (Table 1).

The reference hardening curve for the direct identification method is obtained from the experimental stress-strain relationship until plastic instability. The reference for the inverse approach is identified by updating the material data such as A, B, C and K-value during the finite element simulations to reduce the load errors vs. axial length variation in both the tensile bar and the compressive elliptical cylinder. The k-parameter values obtained for each yielding surface at a specific plastic work are given in Table 2. Note that the evolution of this value k with the specific plastic work for the different identification approaches (Fig. 2) also depends on the strain hardening coefficients, particularly on the stress stagnation B and strain hardening rate C (Table 2).

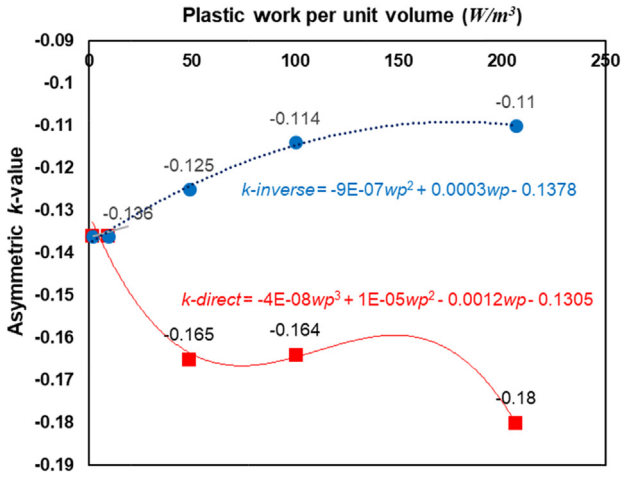

Fig. 2 – Tension compression asymmetry k-value of CPB06 identified from direct and inverse approaches.

3. Prediction assessment of the calibration approaches

For assessing the calibration approaches, tensile loadings on a cylindrical bar (Fig. 3a) and sheet sample are simulated. Under compression, numerical results are given from the elliptical cylinder (Fig. 3c). The FE code LAGAMINE developed at the University of Liège since 1985 is used to simulate the experiments [39–42]. The dimensions and meshing of the samples are detailed in Fig. 3. Each sample has a particular model prediction application or purpose. Tensile is generally required for drawing processes, sheet samples under plane strain tensile for sheet metal forming applications and compression for forging operations. The computed and analyzed simulations results include equivalent plastic strain fields, sample shapes, and total loading force evolution with axial displacement.

3.1. *Tensile and compressive loading predictions*

The results obtained for the tensile of the cylindrical bar and compression of the elliptic cylinder, both axially loaded in the reference direction, are shown in Fig. 4. At the same time, the prediction errors for each identification approach are given in Table 3. The prediction capabilities of the two models have also been tested in cylindrical bars with 6 different notches providing both error predictions lower than 3%. The maximum discrepancies are found for the model calibrated with the direct strategy, with a 31% model prediction error for the load and 23% for the displacement field in the cylindrical tensile bars (CPB06-direct in Fig. 4a). However, in this sample, the predictions of load and shape are accurate for the inversely identified CPB06 model (CPB06-inverse), from initial plasticity until the onset of necking. An increasing prediction error is found until just before fracture but with values lower than 6% for both the loading and displacement fields. To understand this significant difference, we must analyze the data used for each strategy and the requirements for data predictions of each sample in terms of strain values. As the stress computation data (CPB06-direct) have been identified by considering the Considère criterion for accurate stress computation excluding plastic instability and non-uniaxial stress, the material behavior from strain values higher than 10% is not an input. This is not an issue for the notch samples with a high triaxiality as these samples reach strains of only low values, and both identified data sets include these material data. The inverse identification method of the tensile-compression asymmetry parameter (k) and strain hardening law coefficients (A, C, and D) provides the model with an improved prediction of axial loading both over the entire

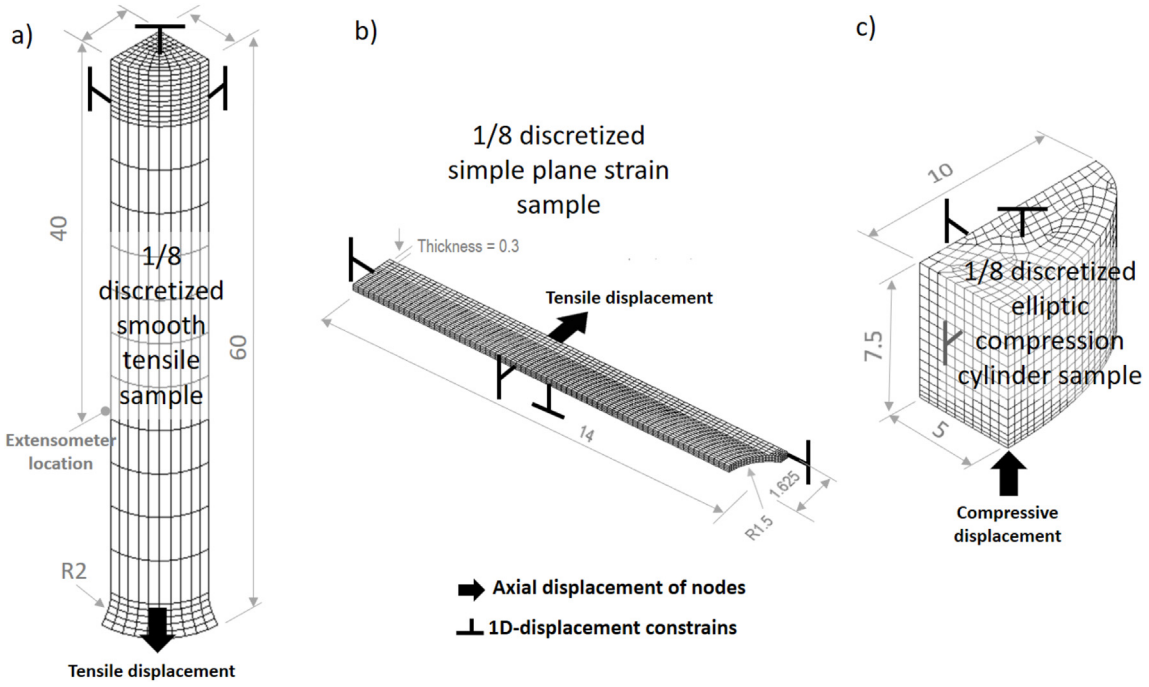

Fig. 3 – Samples meshing including fixations and displacements from machine loadings: (a) tensile, (b) plane strain and (c) compression sample.

elongation range of cylindrical tensile specimens and up to 95% of the axial compressive strain (Fig. 4c). For the case of tensile loading of cylindrical specimens, the model identified by the inverse strategy not only correctly describes the onset of plasticity and hardening, but also ensures a correct prediction of the plastic instability up to just before the maximum fracture strain. Even if complex strain hardening models are available for extrapolating the stress-strain relationship after the onset of necking, taking instability data into account can significantly reduce the complete nonlinear plasticity model prediction errors by around 20%.

3.2. *Analysis of plane – strain predictions*

For the case of simple plane strain, both strategies yield accurate results, with a slightly better prediction for CPB06-inverse (Fig. 4b). The low average strain value (0.11) reached at the maximum elongation of the plane strain tensile sample (Fig. 5) explains this result, which is close to the plastic instability value in the uniaxial tensile test. Additionally, the results obtained by CPB06-inverse indicate that the load evolving is more uniformly distributed with the increase in strain than CPB06-direct. Localized values of 0.2 strain in the center of the sample (Fig. 5) indicate a local thickness reduction with high triaxiality which consequently reduces its load-bearing capacity prior to fracture. Considering the overall plastic strain in the sample, around 90% reached a maximum strain of 0.1. This strain value is close to the onset of plastic instability, indicating that prior deformation follows the high accuracy of the two identification approaches (Fig. 4a and b).

3.3. *Discussion on the identification strategies and their effect on model predictions*

These findings are supported by the results obtained by Tuninetti et al. [25], who evaluated the quasi-static mechanical response of a Ti64 alloy by analyzing the asymmetry. They pointed out the sensitivity of the inverse method to high-strain distribution. Consequently, the solution obtained through the inverse method is smoother and continuously differentiable, resulting in higher accuracy and stability. On the other hand, the CPB06-direct method may require a greater number of nodes and placement points to obtain an accurate solution, which may influence the accuracy.

In contrast, the CPB06-inverse method may require fewer nodes and collocation points, resulting in an efficient solution with a lower computational cost. These results are supported and explained in previous proceeding work [38], where experimental load-elongation curves in tension and compression were evaluated, obtaining a better fit for the CPB06-inverse method using the experimental results from the instability point until rupture. The results obtained in Ref. [38] are also supported by Tu et al. [43], who described the inverse identification method as providing high accuracy by properly verifying the strain hardening rules in the material. CPB06, with the direct strategy, provides evidence of the significant difficulty encountered by several authors in predicting large deformations after the triaxiality point using the Bridgman correction method (Fig. 6).

The analysis developed by Tu et al. [43] concluded that the correction method needed to be more suitable for large displacements. Based on the above, the finding of this work

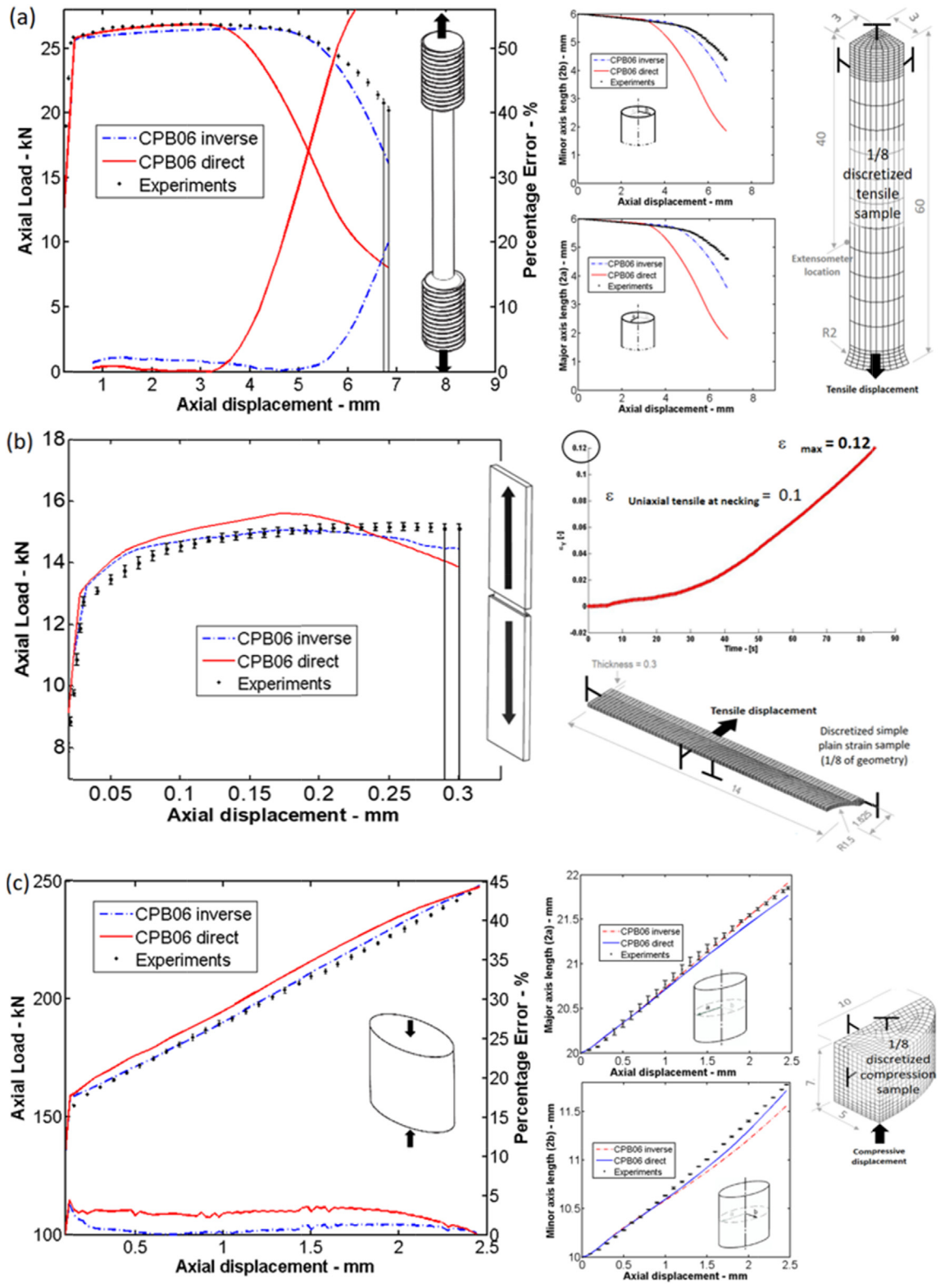

Fig. 4 – Load (F) and cross-sectional area: model predictions from direct and inverse methods with experiments. Tensile testing of (a) bar including plastic instability and (b) plane-strain samples. (c) Elliptical cylinder under compression.

concerning the inverse method solves this problem of plastic flow range in hcp materials, enabling its use in large plastic deformation processes such as metal forming.

This study allows confirming that to increase the accuracy of load and transverse area predictions during plastic deformation of the Ti64 until fracture, asymmetrical hardening

Table 3 – Root mean square model prediction error for each loading condition and global value.

Method	Plane strain	Compression		Tensile		Global
	Load	Load	Shape	Load	Shape	
Direct	4%	3%	0.5%	31%	23%	12%
Inverse	2%	1%	0.6%	6%	5%	3%

parameter k should be identified for values of plastic work higher than the values reached at the onset of necking, or stress-strain curves until 0.1 (CPB06 direct). The prediction accuracy of the load and shape just before fracture in cylindrical tensile test were increased by identifying a new set of hardening parameters and k values with inverse modeling. Higher accuracy increases the load predictions in the samples with higher stress triaxilities while simultaneously reducing the shape prediction errors in notched bars. Finally, to increase the prediction of mechanical deformation of Ti64 in specimens with several combined stress states and high stress triaxilities, the asymmetric anisotropic pressure sensitive plasticity-damage model is required [44], especially for accurate prediction of sheet metal forming and forming limit diagrams [45].

These findings highlight the importance of carefully selecting the appropriate modeling method and parameters to ensure accurate and efficient predictions in plastic deformation scenarios. Both the CPB06-direct and CPB06-inverse methods yield accurate results for simple plane strain, with a slightly better prediction for CPB06-inverse. However, the CPB06-direct method may require a more significant number of nodes and placement points to obtain an accurate solution, which may influence the accuracy. Therefore, it is important to consider the trade-off between accuracy and computational

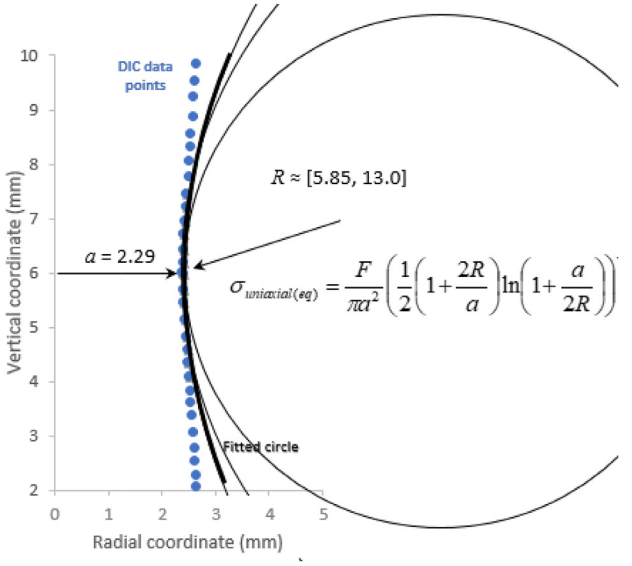

Fig. 6 – Experimental neck of the tensile cylinder at maximum elongation showing difficulties in accurately measuring the radius (R) required to apply the Goodman corrector.

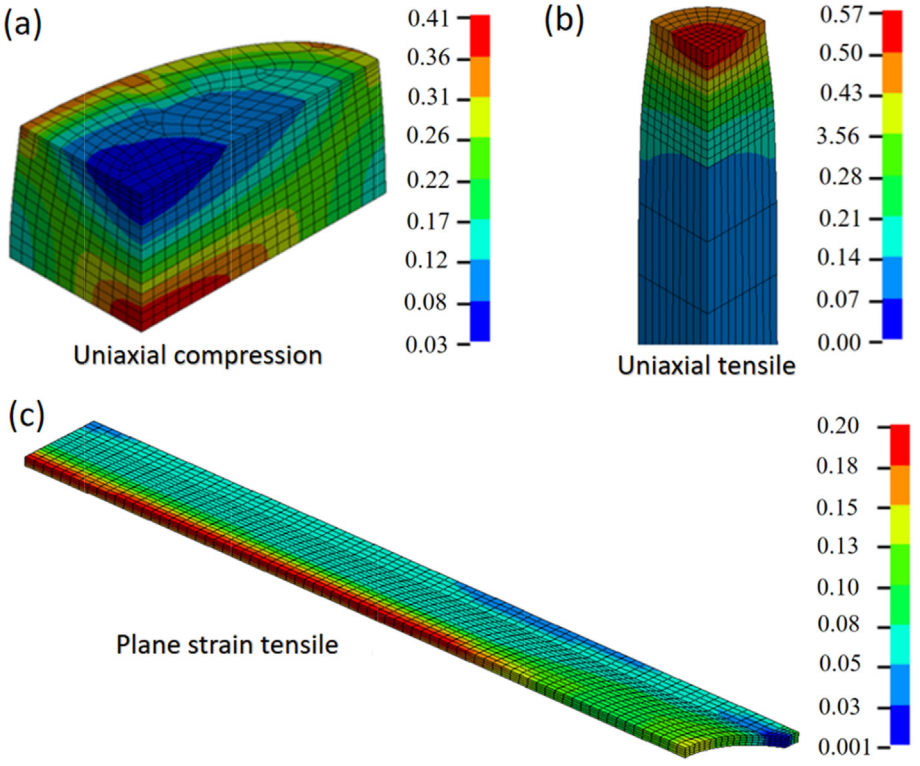

Fig. 5 – Contour plot for the equivalent strain of the investigated samples, noting maximum values reached are: 95% of the maximum axial fracture deformation for (a) compressive sample and at the onset of fracture for tensile loadings: (b) uniaxial, and (c) plane strain.

cost when selecting the appropriate modeling method and parameters for a given plastic deformation scenario.

4. Conclusions

The influence of the direct and inverse strategies on the asymmetric prediction of plastic flow at large deformations using the CPB06 plasticity model has been studied in this work. The difficulty in predicting the plastic behavior of hcp Ti64 alloy is not only due to its inherent slip systems and plasticity governing mechanisms which are well described by the CPB06 model, but also by the chosen calibrations approaches, which significantly affect the quality of the model predictions. The conclusions established in this work are listed below.

- The CPB06 criterion is suitable for modeling the asymmetry behavior due to slip and twinning planes in hcp Ti64 alloy above the triaxial instability point and reaching strains close to the fracture point.
- The model identified with the direct strategy exhibits considerable errors in predicting the post-necking area of the axially loaded cylindrical bar. This is mainly due to the stress stagnation feature of the Voce model; however, the finding confirms that the finite element-based inverse strategy is essential to accurately describe the large deformation behavior in the triaxial state with plastic instability for the investigated model.
- The use of inverse identification is recommended for accurately calibrating models of hcp alloys with restricted slip planes and complex flow behavior such as asymmetric tension/compression strain hardening at large deformations including plastic instability and fracture loads. In the case of Ti64 alloy, the overall prediction error is less than 3%.

Declaration of competing interest

The authors declare that they have no known competing financial interests or personal relationships that could have appeared to influence the work reported in this paper.

Acknowledgments

This research received no funding.

REFERENCES

[1] Biyik S, Aydin M. Optimization of mechanical alloying parameters of Cu25W electrical contact material. Acta Phys Pol, A 2017;132:909–12. https://doi.org/10.12693/APhysPolA.132.909.
[2] Biyik S, Aydin M. The effect of milling speed on particle size and morphology of Cu25W composite powder. Acta Phys Pol, A 2015;127:1255–60. https://doi.org/10.12693/APhysPolA.127.1255.
[3] Biyik S. Effect of polyethylene glycol on the mechanical alloying behavior of Cu-W electrical contact material. Acta Phys Pol, A 2018;134:208–12. https://doi.org/10.12693/APhysPolA.134.208.
[4] Biyik S. Influence of type of process control agent on the synthesis of Ag8ZnO composite powder. Acta Phys Pol, A 2019;135:778–81. https://doi.org/10.12693/APhysPolA.135.778.
[5] Jardin RT, Tuninetti V, Tchuindjang JT, Duchêne L, Hashemi N, Tran HS, et al. Optimizing laser power of directed energy deposition process for homogeneous AISI M4 steel microstructure. Opt Laser Technol 2023;163:109426. https://doi.org/10.1016/j.optlastec.2023.109426.
[6] Bustos F, Hinojosa J, Tuninetti V. Computational comparison of performance of different steel plate shear yielding dampers. Buildings 2023;13:793. https://doi.org/10.3390/buildings13030793.
[7] Azpiazu LE, Egea A, Letzig D, Ha C. Advanced direct extrusion process with real-time controllable extrusion parameters for microstructure optimization of magnesium alloys. Int J Material Form 2023;16:1–8. https://doi.org/10.1007/s12289-023-01758-z.
[8] Güler O, Varol T, Alver Ü, Biyik S. The wear and arc erosion behavior of novel copper based functionally graded electrical contact materials fabricated by hot pressing assisted electroless plating. Adv Powder Technol 2021;32:2873–90. https://doi.org/10.1016/j.apt.2021.05.053.
[9] Biyik S. Characterization of nanocrystalline Cu25Mo electrical contact material synthesized via ball milling. Acta Phys Pol, A 2017;132:886–8. https://doi.org/10.12693/APhysPolA.132.886.
[10] Biyik S. Effect of cubic and hexagonal boron nitride additions on the synthesis of Ag–SnO 2 electrical contact. Material. J Nanoelectron Optoelectron 2019;14:1010–5. https://doi.org/10.1166/jno.2019.2592.
[11] Racz SG, Breaz RE, Tera M, Gîrjob C, Biriș C, Chicea AL, et al. Incremental forming of titanium Ti6Al4V alloy for cranioplasty plates—decision-making process and technological approaches. Metals 2018;8. https://doi.org/10.3390/met8080626.
[12] Tian Y, Hu H, Zhang D. A novel severe plastic deformation method for manufacturing Al/Mg bimetallic tube. Int J Adv Manuf Technol 2021;116:2569–75. https://doi.org/10.1007/s00170-021-07513-5.
[13] Dilberoglu UM, Gharehpapagh B, Yaman U, Dolen M. Current trends and research opportunities in hybrid additive manufacturing. Int J Adv Manuf Technol 2021;113:623–48. https://doi.org/10.1007/s00170-021-06688-1.
[14] Biyik S, Arslan F, Aydin M. Arc-erosion behavior of boric oxide-reinforced silver-based electrical contact materials produced by mechanical alloying. J Electron Mater 2015;44:457–66. https://doi.org/10.1007/s11664-014-3399-4.
[15] Biyik S, Aydin M. Fabrication and arc-erosion behavior of Ag8SnO2 electrical contact materials under inductive loads. Acta Phys Pol, A 2017;131:339–42. https://doi.org/10.12693/APhysPolA.131.339.
[16] Biyik S. Effect of reinforcement ratio on physical and mechanical properties of Cu-W composites synthesized by ball milling. Mater Focus 2018;7:535–41. https://doi.org/10.1166/mat.2018.1513.
[17] Kotzem D, Arold T, Bleicher K, Raveendran R, Niendorf T, Walther F. Ti6Al4V lattice structures manufactured by electron beam powder bed fusion - microstructural and mechanical characterization based on advanced in situ techniques. J Mater Res Technol 2023;22:2111–30. https://doi.org/10.1016/j.jmrt.2022.12.075.
[18] Sabard A, McNutt P, Begg H, Hussain T. Cold spray deposition of solution heat treated, artificially aged and naturally aged Al 7075 powder. Surf Coating Technol 2020;385:125367. https://doi.org/10.1016/j.surfcoat.2020.125367.

[19] Rojas-Ulloa C, Bouffioux C, Jaramillo AF, García-Herrera CM, Hussain T, Duchêne L, et al. Nanomechanical characterization of the deformation response of orthotropic Ti–6Al–4V. Adv Eng Mater 2021;23:2001341. https://doi.org/10.1002/adem.202001341.
[20] Xiao G, Xia Q, Zhang Y, Cheng X. Manufacturing of Ni-based superalloy thin-walled components by complex strain-path spinning combined with solution heat treatment. Int J Adv Manuf Technol 2021;117:199–215. https://doi.org/10.1007/s00170-021-07676-1.
[21] Oñate A, Sanhueza JP, Zegpi D, Tuninetti V, Ramirez J, Medina C, et al. Supervised machine learning-based multi-class phase prediction in high-entropy alloys using robust databases. J Alloys Compd 2023;962:171224. https://doi.org/10.1016/j.jallcom.2023.171224.
[22] Bambach M, Sizova I, Sydow B, Hemes S, Meiners F. Hybrid manufacturing of components from Ti-6Al-4V by metal forming and wire-arc additive manufacturing. J Mater Process Technol 2020;282:116689. 10.1016/j.jmatprotec.2020.116689.
[23] Huang W, Chen X, Huang X, Wang H, Zhu Y. Anisotropic study of Ti6Al4V alloy formed by selective laser melting. J Occup Med 2021;73:3804–11. https://doi.org/10.1007/s11837-021-04765-0.
[24] Tuninetti V, Jaramillo AF, Riu G, Rojas-Ulloa C, Znaidi A, Medina C, et al. Experimental correlation of mechanical properties of the Ti-6Al-4V alloy at different length scales. Metals 2021;11:104. https://doi.org/10.3390/met11010104.
[25] Tuninetti V, Gilles G, Milis O, Pardoen T, Habraken AM. Anisotropy and tension–compression asymmetry modeling of the room temperature plastic response of Ti–6Al–4V. Int J Plast 2015;67:53–68. https://doi.org/10.1016/j.ijplas.2014.10.003.
[26] Kowalczyk-Gajewska K, Sztwiertnia K, Kawałko J, Wierzbanowski K, Wronski M, Frydrych K, et al. Texture evolution in titanium on complex deformation paths: experiment and modelling. Mater Sci Eng, A 2015;637:251–63. https://doi.org/10.1016/j.msea.2015.04.040.
[27] Jia Y, Bai Y. Experimental study on the mechanical properties of AZ31B-H24 magnesium alloy sheets under various loading conditions. Int J Fract 2016;197:25–48. https://doi.org/10.1007/s10704-015-0057-7.
[28] Zhang K, Badreddine H, Yue Z, Hfaiedh N, Saanouni K, Liu J. Failure prediction of magnesium alloys based on improved CDM model. Int J Solid Struct 2021:217–8. https://doi.org/10.1016/j.ijsolstr.2021.01.013.
[29] Lee H, Jo M, Noh G. Biomechanical effects of dental implant diameter, connection type, and bone density on microgap formation and fatigue failure: a finite element analysis. Comput Methods Progr Biomed 2021;200:105863. https://doi.org/10.1016/j.cmpb.2020.105863.
[30] Wu S-H, Song N-N, Andrade Pires FM, Santos AD. Prediction of forming limit diagrams for materials with HCP structure. Acta Metall Sin (English Lett 2015;28:1442–51. https://doi.org/10.1007/s40195-015-0344-3.
[31] Harbaoui Rym, Daghfas Olfa, Znaidi Amna, Tuninetti Victor. Mechanical behavior of materials with a compact hexagonal structure obtained by an advanced identification strategy of HCP material, AZ31B-H24. Frat. Ed Integrità Strutt 2020;14:295–305. https://doi.org/10.3221/IGF-ESIS.53.23.
[32] Jedidi MY, Ben Bettaieb M, Abed-Meraim F, Khabou MT, Bouguecha A, Haddar M. Prediction of necking in HCP sheet metals using a two-surface plasticity model. Int J Plast 2020;128:102641. https://doi.org/10.1016/j.ijplas.2019.102641.
[33] Williams BW, Boyle KP. Characterization of anisotropic yield surfaces for titanium sheet using hydrostatic bulging with elliptical dies. Int J Mech Sci 2016;114:315–29. https://doi.org/10.1016/j.ijmecsci.2016.05.022.
[34] Kakogiannis D, Verleysen P, Belkassem B, Coghe F, Rabet L. Multiscale modelling of the response of Ti-6AI-4V sheets under explosive loading. Int J Impact Eng 2018;119:1–13. https://doi.org/10.1016/j.ijimpeng.2018.04.008.
[35] Tuninetti V, Gilles G, Flores P, Pincheira G, Duchêne L, Habraken A-M. Impact of distortional hardening and the strength differential effect on the prediction of large deformation behavior of the Ti6Al4V alloy. Meccanica 2019;54:1823–40. https://doi.org/10.1007/s11012-019-01051-x.
[36] Cazacu O, Revil-Baudard B, Chandola N. Plasticity-damage couplings: from single crystal to polycrystalline materials, 253; 2019.
[37] Tuninetti V, Flores P, Valenzuela M, Pincheira G, Medina C, Duchêne L, et al. Experimental characterization of the compressive mechanical behaviour of Ti6Al4V alloy at constant strain rates over the full elastoplastic range. Int J Material Form 2020. https://doi.org/10.1007/s12289-020-01543-2.
[38] Tuninetti V, Gilles G, Sepúlveda H, Pincheira G, Flores P, Duchêne L, et al. Direct and inverse characterization of the asymmetric hardening behavior of bulk Ti64 alloy. Basel Switzerland: ICEM 2022; 2022. p. 2. https://doi.org/10.3390/psf2022004002. MDPI.
[39] Yuan S, Duchêne L, Keller C, Hug E, Folton C, Betaieb E, et al. Mechanical response of nickel multicrystals for shear and tensile conditions at room temperature and 573 K. Mater Sci Eng, A 2021;809:140987. https://doi.org/10.1016/j.msea.2021.140987.
[40] Yuan S, Duchêne L, Keller C, Hug E, Habraken A-M. Tunable surface boundary conditions in strain gradient crystal plasticity model. Mech Mater 2020;145:103393. https://doi.org/10.1016/j.mechmat.2020.103393.
[41] MSM & GEG (ULiege). Lagamine software. Univ Liege; 2022. http://www.lagamine.uliege.be/dokuwiki/doku.php. [Accessed 15 June 2023].
[42] Cescotto S, Charlier R. Frictional contact finite elements based on mixed variational principles. Int J Numer Methods Eng 1993;36:1681–701. https://doi.org/10.1002/nme.1620361005.
[43] Tu S, Ren X, He J, Zhang Z. Stress–strain curves of metallic materials and post-necking strain hardening characterization: a review. Fatig Fract Eng Mater Struct 2020;43:3–19. https://doi.org/10.1111/ffe.13134.
[44] Rojas-Ulloa C, Valenzuela M, Tuninetti V, Habraken AM. Identification and validation of an extended Stewart-Cazacu micromechanics damage model applied to Ti–6Al–4V specimens exhibiting positive stress triaxialities. Proc Inst Mech Eng Part L J Mater Des Appl 2021;235:1248–61. https://doi.org/10.1177/14644207211009933.
[45] Singh A, Basak S, Lp PS, Roy GG, Jha MN, Mascarenhas M, et al. Prediction of earing defect and deep drawing behavior of commercially pure titanium sheets using CPB06 anisotropy yield theory. J Manuf Process 2018;33:256–67. https://doi.org/10.1016/j.jmapro.2018.05.003.